A Theory of Low-Frequency Combustion Instability in Solid Rocket Motors

ROBERT SEHGAL* AND LEON STRAND†
Jet Propulsion Laboratory, California Institute of Technology, Pasadena, Calif

A theoretical investigation of low-frequency combustion instability is conducted where the mechanism of instability is the lag of burning-rate response to pressure disturbances near the propellant surface due to the temperature gradient just below the surface and its interaction with lag in exhausting the chamber due to nozzle flow The period of low-frequency chamber fluctuations is considered large compared to any time lags in the gas-phase burning process The burning-rate perturbations and pressure perturbations are related through a closed-loop feedback system analysis The burning-rate fluctuations cause pressure fluctuations through the chamber transfer function These pressure fluctuations are, in turn, fed back to the burning-rate fluctuations through the combustion transfer function Expressions are derived for the two transfer functions, and an instability criterion is developed by the application of Cauchy's theorem, resulting in the correlation of the critical pressure for a given propellant and chamber characteristic length L^* The results are compared with experimental data obtained at the Jet Propulsion Laboratory

Nomenclature

A = parameter defined in equation
A_1 A_2 = undetermined coefficients
A_b = burning area, cm²
A_t = nozzle throat area, cm²
a = constant in de Saint-Robert's law
B = frequency factor, cm/sec
C = E/RT_s
C_D = discharge coefficient, 1/sec
c_p = constant pressure specific heat of solid phase, cal/g/°K
E = activation energy, cal/mole
F = feedback term defined in Eq (38)
G_1 = chamber transfer function
mG_2 = combustion transfer function
g_2 = transfer function connecting burning-rate perturbation and surface thermal gradient perturbation
H_s = thermal gradient of solid at solid-gas interface
H_+ = thermal gradient of gas at solid-gas interface
K_1, K_2 = proportionality constants
K_3 = constant defined in Eq (13)
k = thermal conductivity of solid, cal/cm/sec/ K
k_g = thermal conductivity of gas phase, cal/cm/sec/°K
L = heat of phase change at surface, cal/g
L^* = characteristic chamber length, cm
M = molecular weight, g/g-mass-mole
$\dot{m}$ = mass transfer rate per unit area, g/cm²/sec
m = mass of gas in chamber, g
n = pressure exponent in de Saint-Robert's law
P = pressure, g/cm/sec²
R = universal gas constant, cal/°K/mole
r = propellant burning rate, cm/sec
S_n = complex variable nondimensionalized by $4\alpha/\bar{r}^2$
s = complex variable, 1/sec
T = temperature, °K
T_f = flame temperature, °K
T_s = surface temperature, °K
T_0 = initial propellant temperature, °K
t = time, sec
V_c = chamber volume, cm³
x = dimension, cm
Z_1, Z_2 = exponents defined in Eq (25)
α = thermal diffusivity, $k/\rho_p c_p$, cm²/sec
β = phase angle
ρ_p = propellant density, g/cm³
ρ_g = density of gaseous products in chamber, g/cm³
τ = chamber time constant, sec
τ_n = chamber time constant, nondimensionalized by $4\alpha/\bar{r}^2$
ω = frequency
ω_r = resonant frequency
η = Laplace transform of surface gradient perturbation
θ = Laplace transform of temperature perturbation
ξ = Laplace transform of burning-rate perturbation
ϕ = Laplace transform of pressure perturbation

Superscript

$\bar{}$ = steady state

Subscripts

c = chamber
s = surface
n = nondimensional
cr = critical

Introduction

FOR the development of low-pressure solid rocket motors, it is desirable to know the lowest pressure stability regions Although extensive work has been done in this area and a complete review is available,[1] [2] none of the past work treats the entire rocket chamber during burning and gives unstable solutions

In this analysis it is considered that a pressure fluctuation near the propellant surface will result at a later instant in a burning-rate fluctuation, the lag in propellant burning-rate response being due to the temperature gradient just below the surface The coupling of this effect with the lag in exhausting the chamber due to nozzle flow is considered to represent the mechanism of instability for low-pressure solid rocket motors This concept was originally advanced by Akiba and Tanno [3] The characteristic time for response to pressure perturbations in the gas phase is assumed to be considerably less than in the solid Thus the period of low-frequency chamber pressure fluctuations is considered large compared to any time lags in the gas-phase reaction process, and the time lag concepts[4] necessitated in other theories between vaporization and combustion are not considered in this

Received September 12, 1963; revision received January 22, 1964 This paper presents the results of one phase of research carried out at the Jet Propulsion Laboratory, California Institute of Technology, under contract NAS 7-100, sponsored by NASA The authors wish to express their appreciation to G Carden of the Jet Propulsion Laboratory for the programming of the equations and many helpful discussions

* Engineering Specialist Associate Fellow Member AIAA
† Research Engineer Associate Member AIAA

study The response mechanism of chamber pressure to a specified burning-rate perturbation and, in turn, the alteration of the burning-rate fluctuation by the fluctuation in pressure are related through a closed-loop feedback system analysis The burning-rate perturbations cause pressure perturbations through chamber transfer function G_1, and the pressure perturbations are, in turn, fed back to the burning-rate perturbations through the combustion transfer function mG_2

Surface Energy Balance

The dependence of burning rate on surface temperature can be expressed by the Arrhenius relationship

$$r = B \exp(-E/RT) \tag{1}$$

The energy balance at the surface can be written as

$$k_g H_+ = k H_s - \rho_p r L \tag{2}$$

Steady-State Conditions

Assuming no reactions within the solid, the conduction of heat in the solid is governed by

$$\partial T/\partial t = \alpha(\partial^2 T/\partial x^2) - r(\partial T/\partial x) \tag{3}$$

Setting the origin of x axis at the propellant surface as shown in Fig 1, the temperature boundary conditions are: for $x = -\infty$, $T = T_0$; for $x = -0$, $T = T_s$; and

$$\partial T/\partial x = H \text{ (thermal gradient at } x = -0) \tag{4}$$

The thermal gradient H is determined by the heat transfer from flame Rewriting Eq (3) for steady-state conditions,

$$\alpha \frac{\partial^2 \bar{T}}{\partial x^2} - \bar{r} \frac{\partial \bar{T}}{\partial x} = \frac{\partial \bar{T}}{\partial t} = 0 \qquad \bar{T} = \bar{T}(x)$$

The partial differentials can be rewritten as total differentials:

$$\frac{d^2\bar{T}}{dx^2} - \frac{\bar{r}}{\alpha}\frac{d\bar{T}}{dx} = 0 \quad \text{or} \quad \frac{d^2\bar{T}}{dx^2} = \frac{\bar{r}}{\alpha}\frac{d\bar{T}}{dx}$$

Solving the differential equation for the preceding boundary conditions,

$$\bar{T} = (\alpha/\bar{r})\bar{H} \exp[(\bar{r}/\alpha)x] + T_0 \text{ at } x = -0;\ \bar{T} = \bar{T} \tag{5}$$

Inserting in Eq (5),

$$\bar{T} = (\alpha/\bar{r})\bar{H} + T_0$$

Substituting for α,

$$k\bar{H} = \rho_p c_p \bar{r}(\bar{T} - T_0) \tag{6}$$

That is, rate of energy increase of propellant equals the rate of heat transferred to the propellant From Eq (2) for steady state

$$k\bar{H}_s = k_g \bar{H}_{s+} + \rho_p \bar{r} L$$

Multiplying through by $\bar{r}$, dividing by $k\bar{H}_s$, and substituting Eq (6),

$$\bar{r} = \frac{\alpha}{k(\bar{T} - T_0)}(k_g \bar{H}_{s+} + \rho_p \bar{r} L) \tag{7}$$

Substituting de Saint-Robert's law $\bar{r} = a\bar{P}^n$ (neglecting erosive burning), Eq (6) can be written as

$$k\bar{H} = \rho_p c_p a^2(\bar{P}^{2n}/\bar{r})(\bar{T} - T_0) \tag{8}$$

Averaged over the time interval pertinent to the low-frequency region considered, the steady-state convective heat-transfer coefficient in the gas-flow boundary layer is assumed constant:

$$k_g \bar{H}_{s+} \alpha (T_f - \bar{T}) \quad \text{or} \quad k_g \bar{H}_{s+} = K_1(T_f - \bar{T}) \tag{9}$$

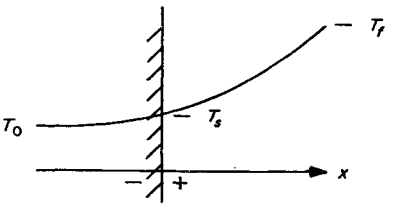

Fig 1 Temperature profile for solid propellant burning

It is also assumed that the steady-state heat transfer in the solid is approximately proportional to the temperature difference in the solid; i e ,

$$k\bar{H}_s = K_2(\bar{T}_s - T_0) \tag{10}$$

where K_1 and K_2 are proportionality constants

Dividing Eq (10) by Eq (9),

$$\frac{k\bar{H}_s}{k_g\bar{H}_+} = \frac{(\bar{T} - T_0)}{(T_f - \bar{T})}\frac{K_2}{K_1} \quad \text{or} \quad k\bar{H} = k_g\bar{H}_{s+}\frac{K_2}{K_1}\left[\frac{(\bar{T} - T_0)}{(T_f - \bar{T})}\right] \tag{11}$$

Substituting Eq (11) into Eq (8),

$$k_g\bar{H}_+\frac{K_2}{K_1}\left[\frac{(\bar{T} - T_0)}{(T_f - \bar{T})}\right] = \rho_p c_p a^2 \frac{\bar{P}^{2n}}{\bar{r}}(\bar{T} - T_0) \tag{12}$$

or

$$k_g\bar{H}_+ = \rho_p c_p a^2(K_1/K_2)(T_f - \bar{T})(P^{2n}/\bar{r})$$

$$k_g\bar{H}_+ = (k/\alpha)a^2(K_1/K_2)(T_f - \bar{T})(P^{2n}/\bar{r})$$

Let

$$(a^2/\alpha)(K_1/K_2) = K_3 \tag{13}$$

$$k_g\bar{H}_+ - k(T_f - \bar{T})(P^{2n}/\bar{r})K_3 \tag{14}$$

Equation (14) explicitly shows the dependence of the gas-phase temperature gradient at the propellant surface on the pressure Substituting Eq (14) into Eq (7),

$$\bar{r} = \frac{\alpha}{k(\bar{T} - T_0)}\left[k(T_f - \bar{T})\frac{P^{2n}}{\bar{r}}K_3 + \rho_p \bar{r} L\right] \tag{15}$$

If one assumes T = const, then $\bar{r}\alpha\bar{P}^n$, which is consistent for the nonerosive burning condition

Nonsteady Problems

Expressing the nonsteady variations in temperature, burning rate, pressure, and surface temperature gradient as small perturbations from steady-state conditions,

$$\begin{aligned} T &= \bar{T} + \theta e^{st} & r &= \bar{r} + \xi e^{st} \\ P &= \bar{P} + \phi e^{st} & H &= \bar{H}_s + \eta e^{st} \end{aligned} \tag{16}$$

where θ, ξ, ϕ, and η are Laplace transform perturbations, functions only of x, and s is a complex variable

Substituting the partial derivatives of Eq (16) into Eq (3) in total differential form,

$$s\theta e^t = \alpha\left[\frac{d^2\bar{T}}{dx^2} + \frac{d^2\theta}{dx^2}e^t\right] - [\bar{r} + \xi e^t]\left[\frac{d\bar{T}}{dx} + \frac{d\theta}{dx}e^t\right] \tag{17}$$

Since ξ and θ are the perturbed values of T and r, their product will be of second order compared to each other and thus can be ignored as a term in the right-hand side of Eq (17)

Separating into steady-state and transient terms, with this assumption, Eq (17) becomes

$$0 = \left[\alpha\frac{d^2\bar{T}}{dx^2} - \bar{r}\frac{d\bar{T}}{dx}\right] + e^t\left[\alpha\frac{d^2\theta}{dx^2} - \bar{r}\frac{d\theta}{dx} - s\theta - \xi\frac{d\bar{T}}{dx}\right] \tag{18}$$

The steady-state condition from Eq (3) is

$$\alpha(d^2T/dx^2) - \bar{r}(d\bar{T}/dx) = 0$$

Thus, Eq (18) simplifies to

$$\alpha \frac{d^2\theta}{dx^2} - \bar{r}\frac{d\theta}{dx} - s\theta = \xi \frac{d\bar{T}}{dx} \tag{19}$$

Differentiating Eq (5) with respect to x yields

$$d\bar{T}/dx = \bar{H} \exp[(\bar{r}/\alpha)x] \tag{20}$$

Then Eq (19) can be written as

$$\alpha \frac{d^2\theta}{dx^2} - \bar{r}\frac{d\theta}{dx} - s\theta = \xi\bar{H} \exp\left(\frac{\bar{r}}{\alpha}x\right) \tag{21}$$

From Eq (16), for $x = 0$,

$$T = \bar{T} + \theta e^{t} = \bar{T}[1 + (\theta/\bar{T})e^{t}]$$

Substituting in Eq (1),

$$r = B \exp\left[-\frac{E}{R\bar{T}[1 + (\theta/\bar{T})e^{t}]}\right]$$

$$r \approx B \exp\left[-\frac{E}{R\bar{T}}\left(1 - \frac{\theta_s}{\bar{T}}e^{t}\right)\right]$$

since $\theta/\bar{T} \ll 1$

By expanding,

$$r = B \exp\left(-\frac{E}{R\bar{T}}\right)\exp\left[\left(\frac{\theta_s}{\bar{T}}\right)\left(\frac{E}{R\bar{T}}\right)e^{t}\right]$$

Using a series expansion for the second exponential, and neglecting all but the first two terms,

$$r = B \exp\left(-\frac{E}{R\bar{T}}\right)\left(1 + \frac{\theta}{\bar{T}}\frac{E}{R\bar{T}}e^{t}\right)$$

$$= \bar{r}\left(1 + \frac{\theta_s}{\bar{T}}\frac{E}{R\bar{T}_s}e^{t}\right) \tag{22}$$

From Eq (16), equating the two equations for r,

$$\bar{r}\left(1 + \frac{\theta}{\bar{T}_s}\frac{E}{R\bar{T}}e^{t}\right) = \bar{r} + \xi e$$

Combining $\bar{r}$ terms and canceling like terms,

$$\bar{r}(\theta/\bar{T})\, E/R\bar{T} = \xi$$

Let $C = E/R\bar{T}$, then

$$\xi = \bar{r}(\theta C/\bar{T}) \quad \text{or} \quad \xi/\bar{r} = C\theta/\bar{T} \tag{23}$$

Rewriting the boundary conditions: for $x = -\infty$, $\theta = 0$; for $x = -0$, $\theta = \theta$; and

$$d\theta/dx = \eta \tag{24}$$

The solution to Eq (21) can be divided into two parts, 1) the homogeneous equation θ_0, and 2) the particular solution θ_p The total solution is

$$\theta = \theta_0 + \theta_p = A_1 e^{Z_1 x} + A_2 e^{Z_2 x} - \frac{\xi\bar{H}}{s}\exp\left(\frac{\bar{r}}{\alpha}x\right) \tag{25}$$

where

$$Z_1 = \frac{\bar{r}}{2\alpha} + \left[\left(\frac{\bar{r}}{2\alpha}\right)^2 + \frac{1}{\alpha}\left(\frac{\bar{r}^2}{4\alpha}\right)S_n\right]^{1/2} = \frac{\bar{r}}{2\alpha}[1 + (1 + S_n)^{1/2}]$$

$$Z_2 = (\bar{r}/2\alpha)\,[1 - (1 + S_n)^{1/2}]$$

and $S_n = (4\alpha/\bar{r}^2)s$, where time is nondimensionalized

The undetermined coefficients A_1 and A_2 can be evaluated from Eq (25) and the boundary conditions

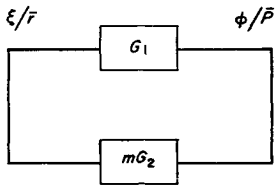

Fig 2 Closed-loop diagram

For $x = (-0)$

$$\theta_{(-0)} = A_1 + A_2 - (\xi\bar{H}/s) = \theta \tag{26}$$

For $x = (-\infty)$

$$\theta_{(-\infty)} = A_1 \exp\left\{\frac{\bar{r}}{2\alpha}[1 + (1 + S_n)^{1/2}](-\infty)\right\} + A_2 \exp\left\{\frac{\bar{r}}{2\alpha}[1 - (1 + S_n)^{1/2}](-\infty)\right\} - \frac{\xi\bar{H}_s}{s}\exp\left(-\frac{\bar{r}}{\alpha}\infty\right) = 0 \tag{27}$$

Since the first and third terms on the right-hand side of Eq (39) are zero, and since the exponent of the second term is >0 because $[1 - (1 + S_n)^{1/2}] < 0$ for all values of $S_n > 0$, in order that $\theta(-\infty) \equiv 0$ for all S_n values, $A_2 \equiv 0$

Equation (26) may be written as

$$A_1 - (\xi\bar{H}/s) = \theta \quad \text{or} \quad A_1 = \theta + (\xi\bar{H}/s) \tag{28}$$

The solution to Eq (21) for any $x < 0$ is

$$\theta_{(x)} = \left[\theta + \frac{\xi\bar{H}}{s}\right]\exp\left\{\frac{\bar{r}}{2\alpha}[1 + (1 + S_n)^{1/2}]x\right\} - \frac{\xi\bar{H}_s}{s}\exp\left(\frac{\bar{r}}{\alpha}x\right) \tag{29}$$

By introducing $d\theta/dx = \eta$ for $x = -0$, the first differential of Eq (29) can be written as

$$\left.\frac{d\theta}{dx}\right|_{x=-0} = \left[\theta + \frac{\xi\bar{H}_s}{s}\right]\left[\frac{\bar{r}}{2\alpha}\right][1 + (1 + S_n)^{1/2}] - \left[\frac{\xi\bar{H}_s}{s}\right]\left[\frac{\bar{r}}{\alpha}\right] = \eta \tag{30}$$

Eliminating θ by using Eq (23), where $\theta = (\xi/\bar{r})\bar{T}/C$

$$\eta = \left[\frac{(\xi/\bar{r})\bar{T}_s}{C} + \frac{\xi\bar{H}_s}{s}\right]\left[\frac{\bar{r}}{2\alpha}\right][1 + (1 - S_n)^{1/2}] - \left(\frac{\xi\bar{H}}{s}\right)\left(\frac{\bar{r}}{\alpha}\right) \tag{31}$$

Again, using the relationship $s = (\bar{r}^2/4\alpha)S_n$, and dividing both sides $(\xi/\bar{r})\bar{H}$, Eq (31) becomes

$$\left[\frac{\eta/\bar{H}_s}{\xi/\bar{r}}\right] = \left[\frac{\bar{T}\bar{r}}{2\alpha C\bar{H}} + \frac{2}{S_n}\right][1 + (1 + S_n)^{1/2}] - \frac{4}{S_n} = \frac{\bar{T}_s\bar{r}}{2\alpha C\bar{H}_s}[1 + (1 + S_n)^{1/2}] + \frac{2}{S_n} \times [(1 + S_n)^{1/2} - 1] \equiv \frac{1}{g_2(s)} \tag{32}$$

where $g_2(s)$ is defined as the transfer function connecting burning-rate perturbations and surface thermal gradient perturbations

Transfer Function of Combustion

The burning-rate perturbations and pressure perturbations are related through a closed-loop feedback system without external inputs, as illustrated in Fig 2 The burning-rate fluctuations cause pressure fluctuations in the chamber

through the chamber transfer function G_1. These pressure fluctuations are, in turn, fed back to the burning-rate fluctuations through the combustion transfer function mG_2.

In terms of input and output, G_1 can be expressed as

$$G_1 = (\phi/\bar{P})/(\xi/\bar{r})$$

Similarly, mG_2 can be expressed as

$$mG_2 = (\xi/\bar{r})/(\phi/\bar{P})$$

Since the reaction time in the gas phase is assumed negligible compared to the solid phase, Eq (14) is assumed to hold without the superscript for low-frequency instability.

From Eq (2) and (14), without the superscript,

$$rkH - \rho_p r^2 L = k(T_f - \bar{T})K_3 P^{2n} \tag{33}$$

Substituting Eq (16) by assuming that

$$r^2 = \left[\bar{r}\left(1 + \frac{\xi}{\bar{r}}e^{t}\right)\right]^2 = \bar{r}^2\left(1 + 2\frac{\xi}{\bar{r}}e^{t} + \quad\right)$$

$$P^{2n} = \left[\bar{P}^{2n}\left(1 + \frac{\phi}{\bar{P}}e^{t}\right)\right]^{2n} = \bar{P}^{2n}\left(1 + \frac{2n\,\phi}{\bar{P}}e^{t} + \quad\right)$$

and utilizing Eq (32), Eq (33) can be written as

$$\frac{\xi}{\bar{r}}e^{t}\left[(\bar{H}\bar{r}k - 2\rho_p L\bar{r}^2) + \frac{\bar{H}\bar{r}k}{g_2(s)} - k(T_f - \bar{T})K_3\bar{P}^2\,\frac{2n\phi/\bar{P}}{\xi/\bar{r}}\right] +$$

$$\bar{H}\bar{r}k - \rho_p L\bar{r}^2 - k(T_f - \bar{T})\,K_3\bar{P}^{2n} = 0 \tag{34}$$

Dividing by $k\bar{H}$, and setting the bracketed term equal to zero, Eq (34) becomes

$$\bar{r}\left(1 - \frac{\rho_p\bar{r}L}{k\bar{H}_s}\right) = \frac{(T_f - \bar{T})K_3\bar{P}^{2r}}{\bar{H}_s} \tag{35}$$

Substituting Eq (35) in the bracketed term,

$$\left[\left(1 - \frac{2\rho_p\bar{r}L}{k\bar{H}}\right) + \frac{1}{g_2(s)} - \left(1 - \frac{\rho_p L\bar{r}}{k\bar{H}}\right)2n\,\frac{\phi/\bar{P}}{\xi/\bar{r}}\right] = 0 \tag{36}$$

Let

$$m = [1 - (\rho_p L\bar{r}/k\bar{H})]2n \tag{37}$$

$$F = [1 - (2\rho_p L\bar{r}/k\bar{H})] \tag{38}$$

But from Eq (6),

$$\frac{\rho_p\bar{r}}{k\bar{H}}L = \frac{L}{c_p(\bar{T} - T_0)}$$

Then

$$F = \left[1 - \frac{2L}{c_p(\bar{T} - T_0)}\right]$$

and

$$m = \left[1 - \frac{L}{c_p(\bar{T} - T_0)}\right]2n$$

Rewriting Eq (36),

$$F + \frac{1}{g_2(s)} - m\,\frac{\phi/\bar{P}}{\xi/\bar{r}} = 0$$

From the transfer-function definition,

$$m\,\frac{\phi/\bar{P}}{\xi/\bar{r}} = \frac{1}{G_2(s)}$$

Then

$$F + \frac{1}{g_2(s)} = \frac{1}{G_2(s)} \tag{39}$$

Chamber Transfer Function

Writing the mass balance equation,

$$\rho_p A_b r = \dot{m}A_t + \frac{d}{dt}(\rho_g V) = P\,A_t\frac{C_D}{g} + \rho_g\frac{dV_c}{dt} + V\,\frac{d\rho_g}{dt} \tag{40}$$

Substituting,

$$\frac{dV_c}{dt} = rA_b \quad \text{and} \quad \frac{d\rho_g}{dt} \approx \frac{M}{RT_f}\frac{dP_c}{dt}$$

$$(\rho_p - \rho_g)rA_b = P\,A_t\frac{C_D}{g} + \frac{MV_c}{RT_f}\frac{dP_c}{dt} \tag{41}$$

Neglecting the gas density compared to the propellant density, and substituting Eq (16), where

$$P = \bar{P} + \phi e^{t} \qquad r = \bar{r} + \xi e^{t}$$

$$dP/dt = (d\phi/dt)e^{t} + s\phi e^{st} = s\phi e^{t}$$

Eq (41) can be written as

$$\frac{\bar{P}}{\bar{r}}(\bar{r} + \xi e^{t}) = \frac{V_c Mg}{C_D RT_f A_t}(s\phi)e^{t} + \bar{P} + \phi e^{t} \tag{42}$$

Simplifying,

$$\frac{\bar{P}}{\bar{r}}\xi = \phi + \frac{V_c Mg}{C_D RT_f A_t}(s\phi)$$

Let

$$\tau = V_c Mg/C_D RT_f A_t \tag{43}$$

Then Eq (43) can be written as

$$(\bar{P}/\bar{r})\xi = \phi[1 + \tau s] \tag{44}$$

Nondimensionalizing s and τ by $4\alpha/\bar{r}^2$, Eq (44) can be written as

$$(\bar{P}/\bar{r})\xi = \phi[1 + \tau_n S_n] \tag{45}$$

Rewriting Eq (45),

$$\frac{\phi/\bar{P}}{\xi/\bar{r}} = G_1 = \frac{1}{1 + \tau_n S_n} \tag{46}$$

Alternate Solution for Chamber Transfer Function

An alternate method of obtaining the chamber transfer function is to write r, P, and dP_c/dt in trigonometric form (Fig 3):

$$r = \bar{r} + \xi\sin(\omega t + \beta)$$

$$P_c = \bar{P} + \phi\sin\omega t$$

$$dp/dt = \phi\omega\cos\omega t$$

where β is a phase angle

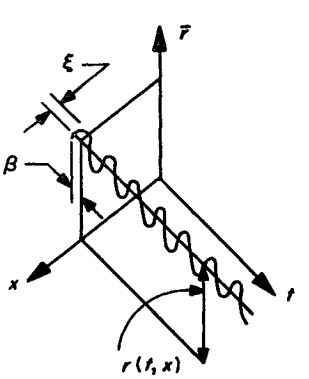

Fig 3 Trigonometric representation of burning rate r

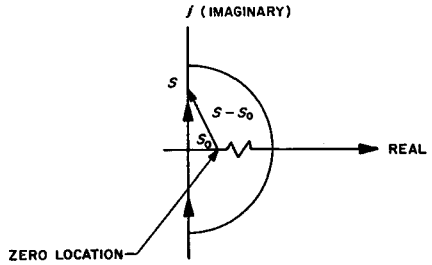

Fig 4 $S - S_0$ locus

Substituting, along with Eq (43), into Eq (41),

$$(\bar{P}/\bar{r})[\bar{r} + \xi \sin(\omega t + \beta)] = \tau_n \phi \omega \cos(\omega t) + \bar{P} + \phi \sin(\omega t)$$

or

$$(\bar{P}/\bar{r})\xi \sin(\omega t + \beta) = \phi(\tau_n \omega \cos\omega t + \sin\omega t) = \phi[(\tau_n\omega)^2 + 1]^{1/2} \sin(\omega t + \beta) \quad (47)$$

where

$$\sin\beta = \frac{\tau_n\omega}{[(\tau_n\omega)^2 + 1]^{1/2}} \quad \text{and} \quad \cos\beta = \frac{1}{[(\tau_n\omega)^2 + 1]^{1/2}}$$

Rewriting Eq (47),

$$\frac{\phi/\bar{P}}{\xi/\bar{r}} = \frac{1}{[(\tau_n\omega)^2 + 1]^{1/2}} \quad (48)$$

This term is the magnitude or amplitude of the chamber transfer function This agrees with the magnitude of $1/(\tau_n S_n + 1)$ That is,

$$\left|\frac{1}{\tau_n S_n + 1}\right| = \left|\frac{1}{\tau_n j\omega + 1}\right| = \frac{1}{[(\tau_n\omega)^2 + 1]^{1/2}}$$

The time constant τ is defined as

$$\tau = \frac{m}{\dot{m}} = \frac{m}{(mRT_f/MV_c)(A_t C_D/g)} = \frac{gV_cM}{RT_fA_tC_D} \text{ (sec)}$$

Low-Frequency Instability

An analysis of the regions of stable and unstable operation of a solid rocket motor is thus reduced to an instability analysis of the closed-loop system From Fig 2, the closed-loop transfer function, by definition,[5] can be written as

$$\frac{\phi/\bar{P}}{\xi/\bar{r}} = \frac{G_1}{1 - mG_1G_2} = \frac{G_1/G_2}{1/G_2 - mG_1} \quad (49)$$

Instability occurs when the denominator of Eq (49) goes to zero, and the transfer function approaches ∞:

$$(1/G_2) - mG_1 = 0 \quad \text{or} \quad mG_1 = 1/G_2$$

Substituting for G_1 and mG_2 from Eqs (46) and (39),

$$F + [1/g_2(s)] = m/(1 + \tau_n S_n) \quad (50)$$

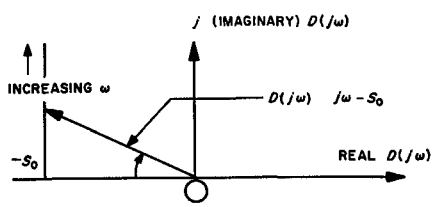

Fig 5 Rotation of $D(j\omega)$ vector

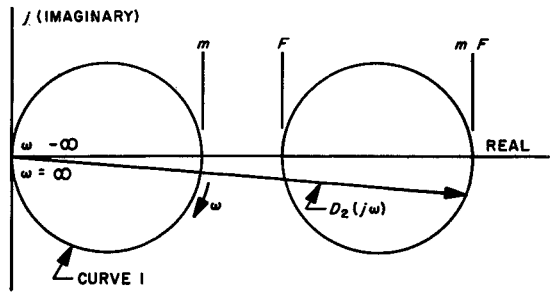

Fig 6 $D_2(j\omega)$ locus on S plane

By making use of Eq (32), Eq (50) becomes

$$\frac{m}{1 + \tau_n S_n} = F + \frac{\bar{T}\bar{r}}{2\alpha C\bar{H}}[1 + (1 + S_n)^{1/2}] + \frac{2}{S_n}[(1 + S_n)^{1/2} - 1]$$

The solution of this equation gives a value of $(\tau_n)_c$ for conditional stability:

$$\frac{m}{(\tau_n)_{cr}S_n + 1} - F = A[1 + (1 + S_n)^{1/2}] + \frac{2}{S_n} \times [(1 + S_n)^{1/2} - 1] \quad (51)$$

where

$$A = \frac{\bar{T}\bar{r}}{2\alpha C\bar{H}} = \frac{\bar{T}_s}{2C(\bar{T}_s - T_0)}$$

Substituting $S_n = (\sigma + j\omega)$ where the resonant frequency ω is nondimensionalized by $4\alpha/\bar{r}^2$ and setting σ equal to zero based on Cauchy's theorem, Eq (51) becomes

$$\frac{m}{1 + j(\tau_n)_c\,\omega} - F = A[(1 + j\omega)^{1/2} + 1] + \frac{2}{j\omega} \times [(1 + j\omega)^{1/2} - 1] \quad (52)$$

where m, F, and A are constants previously determined

Instability Criteria

For the closed-loop transfer function discussed previously, the instability criteria can be determined by the application of Cauchy's theorem,[5] which leads to the condition that the net change in phase going around the closed contour of the over-all function is equal to two times the number of poles minus the number of zeros The locus of a complex number $D(S) = S - S_0$ is determined by plotting the function on a two-component coordinate system with a real and an imaginary axis, as shown in Fig 4, for the case of one zero in the right half of the S plane

As S traces the path shown, the $(S - S_0)$ vector rotates one revolution clockwise as S traces the right-half plane Similarly, for the complex number $D(j\omega) = (j\omega - S_0)$, as $j\omega$ is increased, the vector $(j\omega - S_0)$ rotates one revolution clockwise, as represented in Fig 5 From the Nyquist stability criterion, the system is stable if the vector of $D(j\omega)$

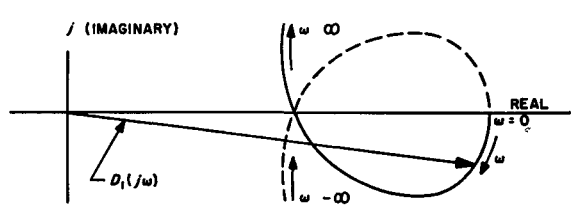

Fig 7 $D_1(j\omega)$ locus on S plane

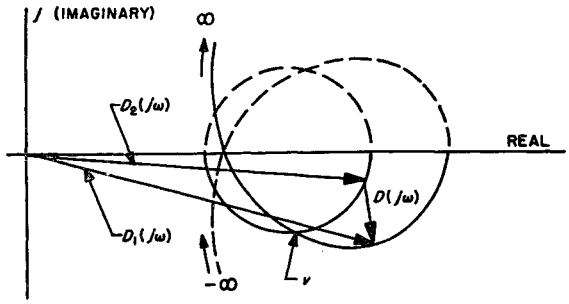

Fig 8 $D(j\omega)$ vector for conditional stability

does not carry out any absolute clockwise revolution about the origin as S travels along its locus

From Eq (50),

$$D(Sn) = D(j\omega) = \frac{1}{g_2(s)} + F - \frac{m}{1 + \tau_n S_n}$$

The vector $D(j\omega)$ can be separated into two components, $D_1(j\omega)$ and $D_2(j\omega)$, such that

$$D(i\omega) = D_1(j\omega) - D_2(j\omega) \qquad (53)$$

where

$$D_1(j\omega) = 1/[g_2(i\omega)]$$

and

$$-D_2(j\omega) = F - \frac{m}{1 + \tau_n j\omega} \quad \text{or} \quad D_2(j\omega) = \frac{m}{1 + \tau_n j\omega} - F$$

Since $m/(1 + \tau_n j\omega)$ is a circle shown as curve 1 in Fig 6, $D_2(j\omega)$ is a circle shifted to the right $-F$ units

From Eq (52) the vector $D_1(j\omega)$ is given by

$$D_1(j\omega) = A[(1 + j\omega)^{1/2} + 1] + \frac{2}{j\omega}[(1 + j\omega)^{1/2} - 1]$$

For $\omega = 0$,

$$D_1(0) = 2A + \frac{2}{j} \lim_{\omega \to 0} \frac{j}{2(1 + j\omega)^{1/2}} = 2A + 1$$

For $\omega = \infty$,

$$D_1(j\omega)|_{\omega = \infty} = A(\infty) + 0 = \infty$$

A typical locus of $D_1(j\omega)$ is shown in Fig 7

Conditional Stability

Figure 8 shows the vector $D(j\omega) = D_1(i\omega) + D_2(j\omega)$ for a conditionally stable condition An intersection of the two curves occurs at point V Whether $D(j\omega)$ has a net clockwise rotation as S traces the right-half plane depends upon whether

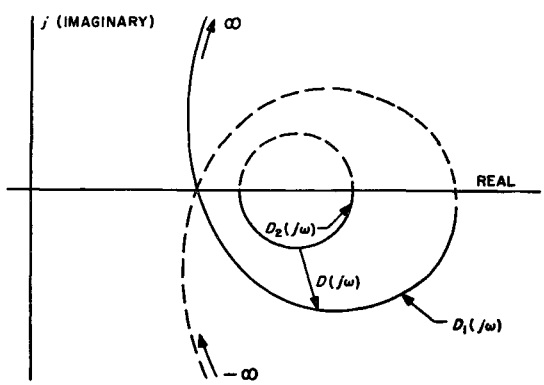

Fig 9 $D(j\omega)$ vector for absolute instability

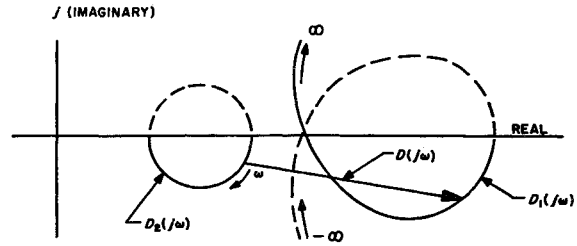

Fig 10 $D(j\omega)$ vector for absolute stability

D_1 or D_2 reaches point V first or simultaneously At the intersection point for positive ω, $D(j\omega)$ equals zero, and the computed resonant frequency and (τ_n) are solutions to Eq (52) for conditonal stability

Absolute Instability and Stability

Absolute instability occurs when $D_1(j\omega)$ begins outside of the circle and no intersection occurs, as shown in Fig 9 For absolute stability, circle $D_2(j\omega)$ is external to, and to the left of, the $D_1(j\omega)$ curve, as shown in Fig 10

Digital Program Outline

A digital program was written to obtain solutions of Eq (52) for conditional stability

Computation of Resonant Frequency ω

From the propellant properties, $m - F$ and $-F$ are calculated, and the $D_2(j\omega)$ circle is located The A parameter is calculated, and the computer then computes the real and imaginary parts of $D_1(j\omega)$ by varying ω in small steps, starting with $\omega = 1$ rad/sec When $D(j\omega)$ crosses the $D_2(j\omega)$ circle, the resonant frequency is computed The computer continues computing $D_1(j\omega)$ for increasing values of ω until

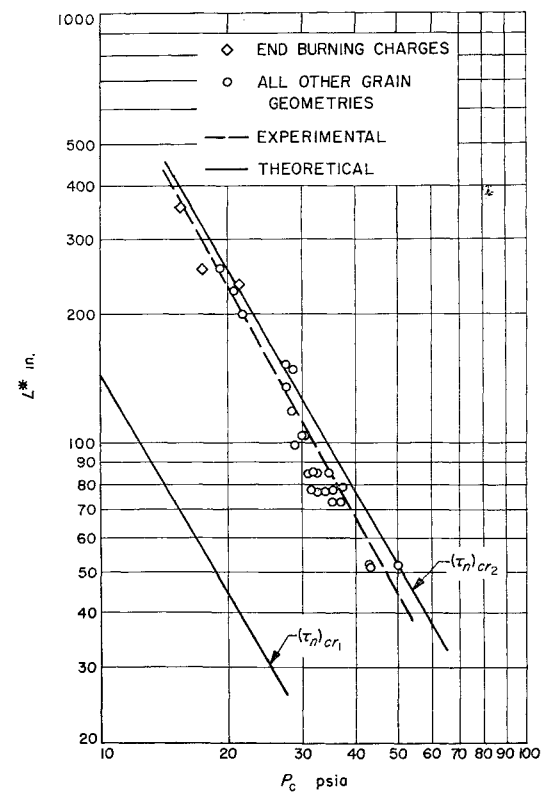

Fig 11 L^* vs pressure for conditional stability; JPL-534 propellant; 80° F

the $D_1(j\omega)$ locus crosses the real axis The crossing frequency and the real component of $D_2(j\omega)$ are determined

Computation of Critical Time Constant $(\tau_n)_c$

The critical time constant is determined by the condition

$$D_2(j\omega\,\tau_n)_c = D_1(j\omega) \tag{54}$$

where the semicircle $D_2(j\omega\tau_n)$ is determined by

$$D_2(j\omega\,\tau_n) = \frac{m}{1 + j\omega\tau_n} - F = \frac{m}{(1 + \omega\tau_n)^2} - \frac{mj\omega\,\tau_n}{(1 + \omega\tau_n)^2} - F \tag{55}$$

Taking real values of Eq (54), and incorporating the real component of Eq (55),

$$\frac{m}{[1 + \omega\,(\tau_n)_c\,]^2} - F = \text{real}[D_1(j\omega)]$$

Solving for $(\tau_n)_c$,

$$(\tau_n)_c = \frac{1}{\omega}\left(\frac{m}{\text{real}[D_1(j\omega)] + F} - 1\right)^{1/2} \tag{56}$$

L^* Correlation

From the definition of (τ_n),

$$(\tau_n)_c = (\tau\,\bar{r}^2/4\alpha) \tag{57}$$

Substituting de Saint-Robert's law and Eq (43) for the time constant, and solving for $V/A_t(L^*)$,

$$L^* = \frac{4\alpha C_D R T_f (\tau_n)_{cr}}{Ma^2 g}\,\bar{P}_c^{-2n} \tag{58}$$

where $\bar{P}_c$ is the critical chamber pressure for conditional stability, and V/A_t is the characteristic chamber length L^* For a given propellant and $(\tau_n)_c$, a log-log plot of L^* vs P should be a straight line with slope equal to $-2n$

Numerical Example

The digital computer program was used to obtain theoretical L^* vs P plots for JPL-534 polyurethane-type propellant The following physical properties were assumed for this propellant:

E/R	= 11,000°K	n	= 0 86
L	= 140 cal/g	C_D	= 6 7 × 10^{-3} l/sec
c_p	= 0 296 cal/g/°K	M	= 24 78 g/g-mole
α	= 2 0 × 10^{-3} cm²/sec	T_0	= 300°K
ρ_p	= 1 69 g/cm³	T	= 905°K
T_f	= 3242°K	a	= 0 00485 in /sec

From the computer calculations, two crossings of the D_1 and D_2 loci were obtained, yielding two values of ω and $(\tau_n)_{cr}$:

ω_1 = 8 31 rad/sec	$(\tau_n)_{c1}$ = 0 209
ω_2 = 22 6 rad/sec	$(\tau_n)_{c2}$ = 1 23

Experimental and theoretical plots of L^* vs P for JPL-534 propellant are shown in Fig 11 This propellant contained 2% aluminum Approximately 40 motors, all designed to burn with a regressive pressure time profile, were fired to study the low-pressure extinction phenomena independent of ignition transients All firings were made near vacuum conditions The theoretical plot was obtained by calculating $\bar{P}_c$ using Eq (58) with the forementioned $(\tau_n)_{cr}$ values and arbitrary L^* values

Additional firings were conducted to investigate the effect of varying aluminum percentage in propellant on the L^* vs extinction pressure relationship [6] It was found that, although the L^* correlation still holds, the negative slope increases with the higher concentrations of aluminum in the propellant and also the extinction pressure at a given L^* The recent window motor studies at the Jet Propulsion Laboratory, with aluminized propellants, strongly suggest the possibility of vapor-phase combustion It seems that radiation plays a significant role; thus, a consideration of this burning phenomenon on the heat transfer to the propellant surface would necessitate modifications to this analysis This investigation is a subject for further research

Conclusions

Based on the concepts advanced by Akiba and Tanno, an analytical model for low-frequency combustion instability has been developed by relating the interaction of burning-rate response to pressure changes due to the temperature gradient in the propellant just below the surface and its interaction with the lag in exhausting the chamber due to nozzle flow A method for obtaining quantitative solutions is outlined by developing a correlation of the critical pressure for a given propellant and chamber characteristic length L^* This correlation gives the theoretical limits of critical chamber pressure where low-frequency combustion instability and ultimate extinction can occur

The parametric studies indicate that resonant frequency is a strong function of surface temperature; therefore, a good knowledge of the physical and ballistic properties of the propellant is required for obtaining this correlation

The case of highly aluminized propellants, where the experimentally observed slope of L^* vs extinction pressure relationship was considerably steeper than predicted theoretically, is an area for further investigation

References

[1] Price, E W, 'Review of experimental research on combustion instability of solid propellants," *ARS Progress in Astronautics and Rocketry: Solid Propellant Rocket Research*, edited by M Summerfield (Academic Press Inc, New York, 1960), Vol I, pp 561–602

[2] Berl, W G, "Combustion instability of solid rocket propellants and motors," Review Paper 2, Solid Propellant Information Agency, Johns Hopkins Univ, Applied Physics Lab, Silver Springs, Md (1962)

[3] Akiba R and Tanno, M, "Low frequency instability in solid rocket motors," *Proceedings of the First Symposium (International) on Rockets and Astronautics* (Tokyo, 1959), pp 74–82

[4] See, for instance, Cheng, S I, "High frequency combustion instability in solid propellant rockets," Jet Propulsion **24**, 27–32, 102–109 (1954)

[5] Fitzgerald, A and Higginbotham, D, *Basic Electrical Engineering* (McGraw-Hill Book Co, Inc, New York, 1957), p 500

[6] Anderson, F, Strehlow, R, and Strand, L, "An experimental investigation of the low pressure combustion limits of some solid propellants," Tech Memo 33-134, Jet Propulsion Lab, Pasadena, Calif (1963)